Structure control of CdS nanobelts and their luminescence properties

Chunrui Wang,[a] K. M. Ip, S. K. Hark, and Quan Li[b]
Department of Physics, The Chinese University of Hong Kong, Shatin, New Territory, Hong Kong, China

(Received 11 August 2004; accepted 7 December 2004; published online 10 February 2005)

Single crystalline CdS (hexagonal) nanobelts have been synthesized using thermal evaporation at temperatures ranging from 1000 to 1200 °C. These nanobelts universally grow along the [120] crystalline direction. The nanobelts fabricated at 1000 °C appear to be much more uniform than those at 1200 °C. Moreover, the surface of the nanobelts grown at 1200 °C is rough compared to that of the former, which is due to the secondary growth of CdS crystallites on the nanobelts' surfaces at higher temperatures, as induced by the surface polarity. Cathodoluminescence and photoluminescence studies disclose the different electronic structure qualities of the two samples. The growth mechanisms of the nanobelts and the luminescence differences of the two samples are discussed. © *2005 American Institute of Physics*. [DOI: 10.1063/1.1852094]

I. INTRODUCTION

Low-dimensional nanosized semiconductors have attracted considerable interest in recent years, as they exhibit strong size-dependent optical and electrical properties, which have potential applications in optoelectronic devices.[1] CdS is one of the most important II-VI semiconductor compounds, possessing excellent optical properties. A tremendous amount of effort has been devoted to the synthesis and optical property study of CdS-related nanoparticles and quantum dots (zero dimension).[2] Recently, a number of groups have fabricated one-dimensional (1D) CdS nanostructures using various chemical or physical methods, including electrochemical deposition,[3] thermal evaporation,[4] solvthermal,[5] surfactant-assisted method,[6] and template.[7] These 1D nanostructures are promising candidates for various nano-optoelectronic devices as they serve as both functional units and wires that connect them. One major concern of using them as building blocks for the nano-optoelectronic devices is the quality of the material's electronic structure, which is important in determining the device efficiency. This becomes particularly important in the case of 1D nanomaterials, where the large surface to volume ratio makes the surface property dominant (which is usually understood as detrimental since surface dangling bonds serve as nonradiactive recombination centers). Unfortunately, such an issue remains controversial in many works due to the lack of detailed experimental data.

In the present study, we report 1D CdS nanobelt growth via thermal evaporation. The nanobelts' surface morphology can be modified by simultaneously inducing secondary growth, which is achieved by varying the processing temperature. These nanobelts (with or without the secondary growth on the surface) demonstrate different luminescence properties, which may relate to their structural differences.

[a]Current address: Department of Physics, Huaibei Coal Industry Teacher's College, Huaibei, 235000 P. R. China; electronic mail: wangcr2001@hotmail.com
[b]Electronic mail: liquan@phy.cuhk.edu.hk

II. EXPERIMENT

The fabrication process is based on thermal evaporation of CdS (sublimation: 980 °C) powders in the absence of any catalyst. Details of the experimental setup can be found elsewhere.[8] The deposition was carried using a high-temperature tube furnace. Two grams of CdS powder (99.99% ARCO) were placed in the center of the tube. The tube was then sealed and pumped down to a base pressure of 2×10^{-2} Torr. Ar was used as the processing gas at a flow rate of 100 sccm. The deposition temperature ranged from 1000 to 1200 °C. The general morphology of the products was examined by scanning electron microscopy (SEM, LEO 1450VP). Powder x-ray diffraction (XRD, Rigaku RU-300 with Cu K_{α_1} radiation) was employed to examine the product's overall crystallinity. Detailed microstructure and chemical composition analysis of individual nanobelts were carried out using a transmission electron microscope (TEM Tecnai 20) equipped with an energy dispersive x-ray (EDX) spectrometer (Oxford Instrument). The room-temperature cathodoluminescence (CL) study of the nanobelts was carried by a MonoCL system with the excitation power at 20 μW (Oxford Instrument) in a scanning electron microscope. Temperature-dependent photoluminescence (PL) spectra were measured from the CdS nanobelts mounted on a cold finger in a continuous cycle cryostat using the 325 nm line of a He-Cd laser. The excitation power density amounts to about 500 W/cm^2, and the emitted light was collected by lenses and dispersed by a 0.75 m Spex 1702 spectrometer equipped with a 1200 l/mm grating. The spectral resolution of the spectrometer was set at 0.6 meV in all measurements.

III. RESULTS AND DISCUSSION

The two samples deposited at 1000 °C (A1 and 1200 °C) (A2) were first examined by SEM. The general morphologies of them appear to be similar at low magnifications [shown in Figs. 1(a) and 1(b)]. Both of them display wire-like nanostructures, and some twisted "wires" demonstrate shape characteristics of nanobelts. Nevertheless, sample A2 is not as uniform as sample A1. There is a large size distribution in sample A2 (nanobelts' width ranges from

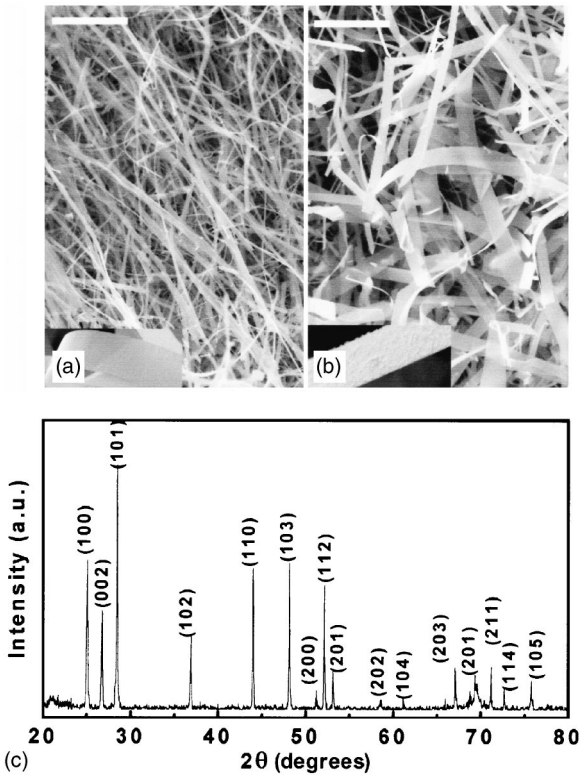

FIG. 1. (a) SEM image of the CdS nanostructures grown at 1000 °C, scale bar: 5 μm. (b) SEM image of the CdS nanostructures grown at 1200 °C, scale bar: 5 μm. (c) Typical XRD spectrum of the CdS nanobelts synthesized with temperatures ranging from 1000 to 1200 °C.

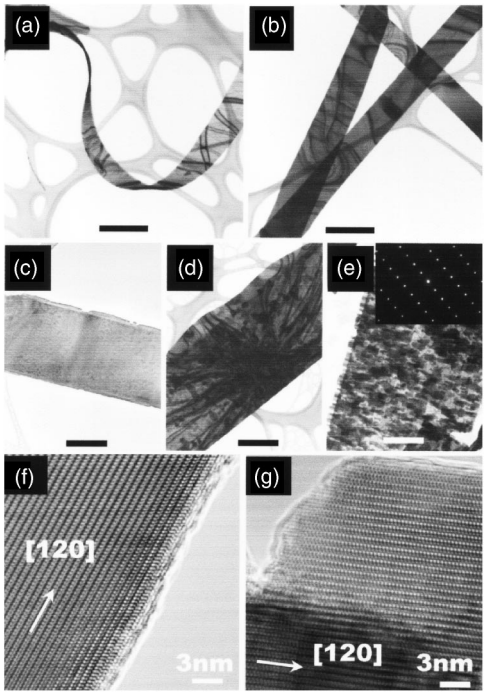

FIG. 2. (a) and (b) Bright-field TEM image of the nanobelts from sample A1 (1000 °C), a smooth nanobelt surface is observed, the contrast results from the bending contours. Scale bar: 500 nm. (c)–(e). Bright-field TEM image of the nanobelts from sample A2 (1200 °C). Scale bar: 500 nm. (f) High-resolution image of sample A1. (g) High-resolution image of sample A2.

hundreds of nanometers to several micrometers), compared to that of sample A1 (width in the range of 200–500 nm). The typical size of sample A2 is much larger than that of A1. Moreover, SEM images of the two samples taken at higher magnifications show distinct difference in the nanobelts' surfaces. While the surface of nanobelt in sample A1 is smooth [in the inset of Fig. 1(a)], it appears to be rough in sample A2 [in the inset of Figure 1(b)]. Although the observation of the nanobelts' morphology in the two samples differs, powder XRD of them give similar results [Fig. 1(c)], in which all of the diffraction peaks can be indexed to those of hexagonal CdS with lattice constant $a=4.136$ Å, and $c=6.713$ Å (JCPDS file No. 77-2306) within the experimental error.

Detailed microstructure analysis from TEM study further confirms the SEM observations. Figures 2(a) and 2(b) show the typical morphology of nanobelts taken from sample A1. They appear to be relative uniform, with a width in the range of 200–500 nm. The fact that the thickness of the nanobelt is much smaller than its width is clearly demonstrated in Fig. 2(a), and average ribbon thickness is less than 20 nm. Transmission electron diffraction (TED) studies (not shown here) of several tens of such nanobelts indicate that all of them are single crystalline, and have a universal growth direction (along the hexagonal [120] direction). Figures 2(c)–2(e) show three nanobelts taken from sample A2. All of them show a light-dark contrast on the sample surface, suggesting larger mass thickness in the dark region. EDX spectra (not shown here) taken from both of the dark and light regions on the nanobelts indicate the same chemical composition (only Cd and S are detected). Nevertheless, the size, shape, and density of these dark regions are different in individual nanobelts, with size ranging from tens to hundreds of nanometers [Figs. 2(c)–2(e)]. Selected-area diffraction pattern in the inset of Fig. 2(e) is taken from the nanobelt shown in the same figure. The diffraction pattern can be indexed to [100] zone axis of hexagonal CdS, and indicates the single crystalline nature of the nanobelt. This is generally observed in tens of such nanobelts examined. Similar to those from sample A1, the nanobelts from sample A2 follow a universal growth direction as well (along [120] direction). The universal growth direction of the nanobelts (A1 and A2) was further confirmed by the high-resolution image. While the terminating surface of sample A1 [Fig. 2(f)] appears to be sharp, the one from sample A2 is rough.

Due to the fact that no metal catalyst was used during the nanobelt growth process, and no particle was observed at the tip of the nanobelts, the formation of the CdS nanobelts may be explained by the vapor-solid mechanism, instead of vapor-liquid-solid mechanism.[9] The sublimed CdS vapor directly deposits at the lower temperature region and grows into belt-like structures. The formation of the belt morphology may be affected by the growth kinetics of different crystalline facets at specific experimental conditions instead of being solely governed by the lowest surface energy argument.[10]

Together with the SEM observations, the dark "particles" on nanobelt surface in the TEM images [Figs. 2(c)–2(e)] are secondary growth (branching) of CdS on the nanobelts. These branches grow directly from the nanobelt surface in the absence of any additional impurity particles. The small branches and the nanobelts have the same crystalline orientation (TED in Fig. 2(e)). The different size, shape,

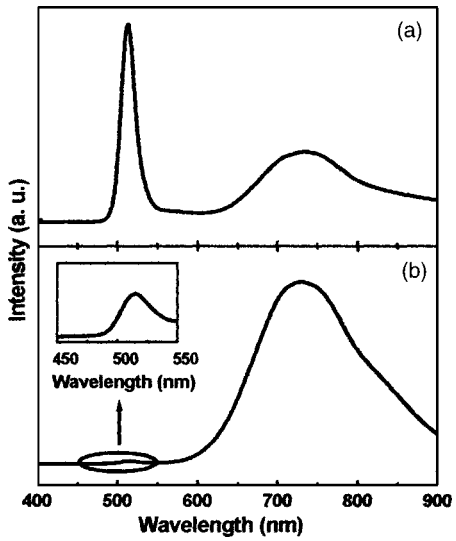

FIG. 3. (a) CL spectrum of sample A1 (1000 °C), displaying a strong green emission and a weak red emission. (b) CL spectrum of sample A2 (1200 °C), displaying a weak green emission and a strong red emission.

and density of these branches suggest different stage of the secondary growth. The branches may coalesce when their lateral size is large enough, which is responsible for the formation of larger and thicker nanobelts in sample A2. Similar phenomena have been reported in several other material systems, including the asymmetric nanocantilever arrays on polar surfaces of ZnO,[11] wurtzite ZnS nanosaw formation,[12] and CdSe nanosaw growth.[13] The asymmetrical growth is more than likely to be induced by the surface polarity of these ionic materials without the center symmetry. Unlike their nanowire counterparts, these nanobelt always extend along the hexagonal $\langle 120 \rangle$ direction, with $\{001\}$ as one of the major termination surfaces, which can be consisted of either a layer of cation (001) or anion $(00\bar{1})$ atoms. The anion-terminated surface $(00\bar{1})$ appears to be chemically inactive, while the metallic clusters (can be Zn or Cd) on the cation-terminated surface (001) or the edge surface $(01\bar{1})$ serve as self-catalysts and promote the secondary growth.[11] This is also consistent with our TEM observations. Moreover, at higher temperature (1200 °C for sample A2), the sublimation rate of CdS is higher compared to that at lower temperature (1000 °C for sample A1). The higher sublimation rate leads to a higher partial pressure of the CdS vapor, and thus a higher supersaturation downstream the tube (due to the temperature gradient of the tube furnace setting), which worsens the nonuniformity of the nanobelts.[14]

The room-temperature cathodoluminescence (CL) spectra of the nanobelts are shown in Fig. 3. The CL spectrum taken from sample A1 [Fig. 3(a)] shows two distinct emission peaks centered at $\simeq$2.4 and $\simeq$1.7 eV, respectively. The intensity of the 2.4 eV peak is higher than the one at 1.7 eV, and its full width at half-maximum (FWHM) smaller. These two emission peaks are also detected in sample A2. However, the intensity ratio $(I_{2.4}/I_{1.7})$ of the two samples changes from 2.76 to 0.01; i.e., the mainly green emission in sample A1 changes to mainly red emission in sample A2. The FWHM of both peaks in sample A2 are larger compared to the corresponding peaks in sample A1.

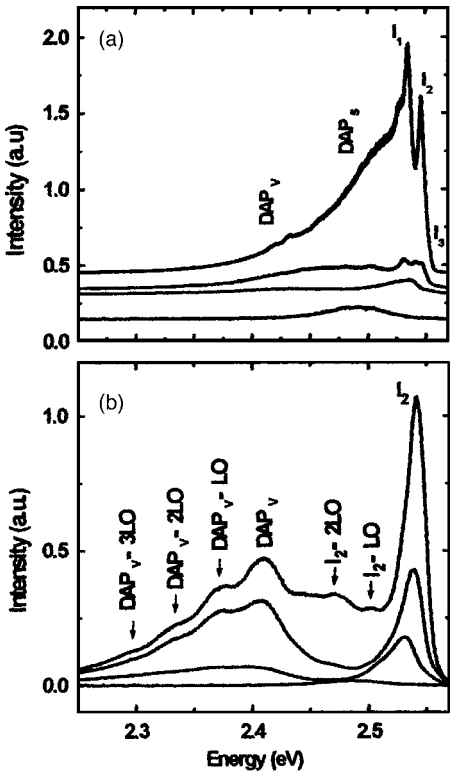

FIG. 4. Temperature-dependent PL spectra of (a) sample A1 and (b) sample A2.

CdS has a direct band gap of 2.42 eV at room temperature.[15] The emission peak at $\simeq$2.4 eV is attributed to the near-band-edge emission,[15,16] and the one at $\simeq$1.7 eV to deep-trap band is related to impurities, native defects, or surface-related defect states.[17–19] The near-band-edge emission may result from the free electron-hole recombination, the shallow-trap state near the band edge, or both. The inhomogeneous broadening of the peaks could be attributed to a high concentration of point defects (defect state overlapping) and/or strain, resulted from more extended defects. The obvious broadening of both emission peaks ($\simeq$2.4 and $\simeq$1.7 eV) observed in sample A2 (compared to sample A1) could be ascribed to the fact that larger crystals tend to harbor more extended defects than small crystals. The ratio changes of the two peaks' intensity $(I_{2.4}/I_{1.7})$ in sample A1 and A2 suggest the increase of the defect states[17] in sample A2. These defects may act at nonradiative recombination centers, which can quench the radiative band edge recombination.[18]

The more detailed electronic structures of the two different types of nanobelts are further disclosed by the temperature-dependent PL spectra, as shown in Fig. 4, where many more peaks of higher energies emerge in the low-temperature spectra than in the room-temperature spectra. At 10 K, the two most intense of these in sample A1 [Fig. 4(a)] are the I_2 peak at 2.540 eV and the I_1 at 2.534 eV, which have been assigned to excitons bound to neutral donors and acceptors.[20] The peak I_3 at 2.550 eV, which is assigned to excitons bound to ionized donors,[21] becomes more obvious in the slightly higher temperature spectra, as donors become increasingly ionized when the temperature rises. As a comparison, fewer features are observed in sample A2. Only

peak I_2 is identified with a much larger peak width, and peak I_1 at 2.534 eV I_3 at 2.550 eV are not seen or unresolved. The phonon replica of peak I_2 is observed at 2.503 eV and 2.474 eV [as marked by arrows in Fig. 4(b)], as CdS are known to exhibit many phonon side bands[22] due to the strong exciton-phonon coupling.

The influence of surface on the PL spectra taken from sample A1 is revealed by the broad asymmetric emission background from $\simeq$2.35 to $\simeq$2.52 eV. Similar emissions had been observed in the PL of thin CdS platelets and identified as originated from surface donor-acceptor pair recombinations (DAP_S).[23] The maximum of the DAP_S emissions is known to shift towards higher energy with increased excitation power density. The confirmation of this in our experiment allowed us to attribute the broad background in our spectra to surface luminescence. Such a surface band disappears in the spectra taken from sample A2, which also explains the observation of phonon replicas of the excitonic emission in sample A2, but not A1.

Small spectral modulations (2.418 and 2.432 eV) on the low-energy tail of DAP_S luminescence is observed in the spectra of sample A1, while a distinct feature at 2.411 eV appears in that of A2, with several phonon replicas on the low-energy tail. These features (in the case of both A1 and A2) are replicated, essentially without any shift, in every spectra obtained below 80 K. They are tentatively attributed to unresolved donor-acceptor pair (DAP_v) emissions within the volume of the nanoribbons.[22]

It is interesting to note that although the thickness of sample A1 is only around 20 nm, the proximity of unpassivated surfaces does not seem to dissociate the excitons. This may be explained by that fact that there are few dangling bonds on the small indice surfaces and the rather tight binding energy of excitons ($\sim$28 meV).[24] Although the size (ribbon thickness) of the same A2 is much larger than that of A1, the electronic structure quality seems to be worse (the larger I_2 peak width and the less resolved excitonic features at high energies). On the other hand, contribution from the surface exists as surface donor-acceptor pair recombination in the luminescence spectra of thin nanoribbons (A1). Such contribution disappears (or become trivial) when the ribbon thickness becomes much larger (hundreds on nanometers due to the secondary growth in sample A2).

IV. CONCLUSION

In conclusion, CdS nanobelts are fabricated by simple thermal evaporation in the absence of any catalyst. These nanobelts appear to be single crystalline with a universal growth direction of [120]. Nevertheless, the CdS nanobelts synthesized at different temperatures appear to have different structural characteristics. The nanobelts grown at 1000 °C appear to be more uniform, and the surfaces of them are smooth, while those at 1200 °C have rough surfaces and a very broad size distribution. This is explained by the secondary growth on the nanobelts surface induced by the surface polarity. Accordingly, the luminescence properties of the samples are different, the nanobelts synthesized at lower temperatures demonstrate higher electronic structure quality compared to those fabricated at high temperature, although their sizes (thickness) are much smaller, and thus the surface effect (usually refers to surface states or surface-related defect states) is expected to be predominant. This finding suggests that the electronic structure quality of the 1D nanomaterials, which eventually determines the nano-optoelectronic device performance, can be good when the material's size is small. The control of the deposition parameter and thus the crystal quality is more important in determining the electronic structure quality of the materials.

ACKNOWLEDGMENT

This research is supported by CERG under project No. CUHK 400904, and RGC direct allocation in the Chinese University of Hong Kong, under project no. 2060261.

[1] A. P. Alivisatos, Science **271**, 933 (1996).
[2] C. W. Litton, D. C. Reynolds, T. C. Collins, and Y. S. Park, Phys. Rev. Lett. **25**, 1619 (1970); A. Blanco, C. Lopez, R. Mayoral, H. Miguez, F. Meseguer, A. Mifsud, and J. Herrero, Appl. Phys. Lett. **73**, 1781 (1998); Y. Kanemitsu, H. Matsubara, and C. W. White, *ibid.* **81**, 535 (2002).
[3] D. Routkevitch, T. Bigioni, M. Moskovitc, and J. M. Xu, J. Phys. C **100**, 14037 (1996); D. S. Xu, Y. J. Xu, D. P. Chen, G. L. Guo, L. L. Gui, and Y. Q. Tang, Adv. Mater. (Weinheim, Ger.) **12**, 520 (2002).
[4] Y. W. Wang, G. N. Meng, L. D. Zhang, C. H. Liao, and J. Zhang, Chem. Mater. **14**, 1773 (2002).
[5] J. H. Zhan, X. G. Yang, D. W. Wang, D. S. Li, Y. Xie, Y. N. Xia, and Y. T. Qian, Adv. Mater. (Weinheim, Ger.) **12**, 1348 (2000).
[6] C. N. R. Rao, A. Gorindaraj, F. L. Deepark, and N. A. Gunari, Appl. Phys. Lett. **78**, 1853 (2001).
[7] M. W. Shao, F. Xu, Y. Y. Peng, J. Wu, Q. Li, S. Y. Zhang, and Y. T. Qian, New J. Chem. **26**, 1440 (2002).
[8] Q. Li and C. R. Wang, Appl. Phys. Lett. **82**, 1398 (2003).
[9] Z. W. Pan, Z. R. Dai, and Z. L. Wang, Science **291**, 1947 (2001).
[10] B. Lewis and J. C. Anderson, *Nucleation and Growth of Thin Films* (Academic, New York, 1978).
[11] Z. L. Wang, X. Y. Kong, and J. M. Zuo, Phys. Rev. Lett. **91**, 185502 (2003).
[12] D. Moore, C. Ronning, C. Ma, and Z. L. Wang, Chem. Phys. Lett. **385**, 8 (2004).
[13] C. Ma, Y. Ding, D. Moore, X. D. Wang, and Z. L. Wang, J. Am. Chem. Soc. **126**, 708 (2004).
[14] R. S. Wagner, *Whisker Technology*, edited by A. P. Levitt (Wiley-Interscience, New York, 1970).
[15] B. G. Yacobi, D. B. Holt, *Cathodoluminescence Microscopy of Inorganic Solids* (Plenum, New York, 1990).
[16] D. Matsuura, Y. Kanemitsu, T. Kushida, C. W. White, J. D. Budai, and A. Meldrum, Appl. Phys. Lett. **77**, 2289 (2000); B. Liu, G. Q. Xu, L. M. Gan, C. H. Chew, W. S. Li, and Z. X. Shen, J. Appl. Phys. **89**, 1059 (2001).
[17] Y. Lin, J. Zhang, E. H. Sargent, and E. Kumacheva, Appl. Phys. Lett. **81**, 3134 (2002); L. Spanhel, M. Haase, H. Weller, and A. Henglein, J. Am. Chem. Soc. **109**, 5649 (1987); M. G. Bawendi, P. J. Carroll, W. L. Wilson, and L. E. Brus, J. Chem. Phys. **96**, 946 (1992).
[18] N. Pinna, K. Weiss, J. Urban, and M. Pileni, Adv. Mater. (Weinheim, Ger.) **13**, 261 (2001).
[19] G. Ma, S. Tang, W. Sun, Z. Shen, W. Huang, and J. Shi, Phys. Lett. A **299**, 581 (2002).
[20] A. Imada, S. Ozaki, and S. Adachi, J. Appl. Phys. **92**, 1793 (2002).
[21] F. T. Vasko and A. V. Kuznetsov, *Electronic States and Optical Transitions in Semiconductor Heterostructures* (Springer, New York, 1999), p. 173.
[22] C. H. Henry, K. Nassau, and J. W. Shiever, Phys. Rev. B **4**, 2453 (1971).
[23] Y. Shiraki, T. Shimada, and K. Konatsubara, J. Phys. Chem. Solids **38**, 937 (1977).
[24] *Landolt-Bornstein Numerical Data and Functional Relationships in Science and Technology*, edited by O. Madelung (Springer, Berlin, 1982), Group III, Vol. 17b, p. 180.